


SCIENTIFIC REPORTS



OPEN

Electronic origins of photocatalytic activity in d^0 metal organic frameworks

Received: 13 November 2015

Accepted: 11 March 2016

Published: 29 March 2016

Maxim A. Nasalevich¹, Christopher H. Hendon², Jara G. Santaclara¹, Katrine Svane², Bart van der Linden¹, Sergey L. Veber^{3,4}, Matvey V. Fedin^{3,4}, Arjan J. Houtepen⁵, Monique A. van der Veen¹, Freek Kapteijn¹, Aron Walsh^{2,6} & Jorge Gascon¹

Metal-organic frameworks (MOFs) containing d^0 metals such as NH₂-MIL-125(Ti), NH₂-UiO-66(Zr) and NH₂-UiO-66(Hf) are among the most studied MOFs for photocatalytic applications. Despite structural similarities, we demonstrate that the electronic properties of these MOFs are markedly different. As revealed by quantum chemistry, EPR measurements and transient absorption spectroscopy, the highest occupied and lowest unoccupied orbitals of NH₂-MIL-125(Ti) promote a long lived ligand-to-metal charge transfer upon photoexcitation, making this material suitable for photocatalytic applications. In contrast, in case of UiO materials, the d -orbitals of Zr and Hf, are too low in binding energy and thus cannot overlap with the π^* orbital of the ligand, making both frontier orbitals localized at the organic linker. This electronic reconfiguration results in short exciton lifetimes and diminishes photocatalytic performance. These results highlight the importance of orbital contributions at the band edges and delineate future directions in the development of photo-active hybrid solids.

Metal-organic frameworks (MOFs) have attracted a great deal of interest during the last decades due to their unprecedented surface area, remarkable tuneability and the fascinating variety of possible combinations of constituting blocks. Several applications have been suggested, such as separation of gases^{1,2}, catalysis³, drug delivery and sensing⁴. Photocatalysis was proposed in the early 2000s inspired by an intuitive analogy between them and their corresponding oxides, often being semiconductors^{5,6}. Despite the fact that the early reports of semiconducting properties of MOFs have been disputed^{7,8}, this initial misconception led to the application of frameworks based on Zn, Ti and other transition metals in a variety of photocatalytic reactions such as oxidation of organic compounds^{9,10}, reduction of metal ions¹¹ and synthesis of solar fuels¹². NH₂-MIL-125(Ti) and NH₂-UiO-66(Zr) clearly stand out as the most researched among the different MOF structures tested in photocatalysis to date. While these two MOFs are based on the same linker and crystallize in a rather similar topology, the metal ions constituting the inorganic nodes in the frameworks are different: Ti⁴⁺ forms octameric Ti₈O₈(OH)₄ rings¹³ in NH₂-MIL-125(Ti) and Zr⁴⁺ or Hf⁴⁺ form the M₆O₄(OH)₄ clusters in the UiOs¹⁴.

Intuitively, the light absorption properties of MOFs are determined by the synergy between the organic ligand and the metal ion. In this case, the addition of the primary amine group to terephthalate alters the electronic properties and promotes absorption in the visible region of the solar spectrum¹⁵. It has been assumed that the three d^0 metals (Ti, Zr and Hf) feature similar electronic properties, accepting electrons in their unoccupied d orbitals. Thus, one would expect that a photo-generated electron in this series of MOFs would result in ligand-to-metal charge transfer (LMCT). Although understanding the nature of the excited states and the redox levels of these MOFs is crucial for the rational design of new photo-active frameworks¹⁶, these important aspects still need to be clarified. The electronic origin of the photocatalytic activity is the focus of this manuscript.

LMCT is generally accepted in the MIL-125(Ti)-type materials and was clearly demonstrated by EPR^{17,18}, flash photolysis¹⁹ and theory²⁰. The highest occupied crystalline orbital (HOCO) of NH₂-MIL-125(Ti) is localized

¹Catalysis Engineering, Department of Chemical Engineering, Delft University of Technology, Julianalaan 136, Delft, The Netherlands. ²Department of Chemistry, University of Bath, Claverton Down, Bath BA2 7AY, UK. ³Laboratory of Magnetic Resonance, International Tomography Center, Institutskaya 3A, Novosibirsk 630090, Russia. ⁴Novosibirsk State University, Novosibirsk 630090, Russia. ⁵Optoelectronic Materials, Department of Chemical Engineering, Delft University of Technology, Julianalaan 136, 2628 BL Delft, The Netherlands. ⁶Department of Materials Science and Engineering, Yonsei University, Seoul, Korea. Correspondence and requests for materials should be addressed to J.G. (email: j.gascon@tudelft.nl)

at the organic linker and the lowest unoccupied crystalline orbital (LUCO) is centred at the Ti *d*-orbitals²¹. Furthermore, the photoexcitation process results in the formation of easily detectable coloured paramagnetic Ti³⁺ species.

The mechanism behind light-excitation in UiO-66(Zr) has been debated by several researchers. Matsuoka and co-workers reported the absence of both photocatalytic activity towards hydrogen evolution and EPR signatures of paramagnetic Zr³⁺ in NH₂-UiO-66(Zr) attributed to the very negative redox potential of Zr⁴⁺-centred clusters¹⁷. In contrast, and in analogy to NH₂-MIL-125(Ti) Li *et al.* and Wang *et al.* ascribed the lowest in energy absorption band to LMCT and reported EPR spectra for this Zr-based MOF as evidence^{9,22,23}.

The LUCO positions determine the ability of these MOFs to perform photo-driven reductions such as H₂ evolution and/or CO₂ reduction. Walsh and co-workers calculated, in line with reported experimental results, that hydrogen evolution is indeed feasible by using X-MIL-125(Ti) because the LUCO potential is more negative than the redox potential of the normal hydrogen electrode (NHE)²⁴. The analysis of the electronic density of states revealed that C, N and O contribute to the HOCO while LUCO is composed of Ti *d* and O *p*-orbitals, indeed in agreement with the EPR results.

This LUCO remains relatively unperturbed by the choice of linkers. Walsh *et al.* reported, based on simple Hammett argument²⁵, that different substituents on the organic linker of MIL-125(Ti) can indeed reduce the band gap down to 1.3 eV for diaminoterephthalate²¹, yet this has little influence on the reductive potential of the excited MOF and is achieved *via* reducing the oxidative potential of the HOCO on the organic linker. In contrast, by changing the metal ions in the inorganic clusters^{23,26}, the reducing potential of MIL-125(Ti) should be changed. For tuning the position of LUCO in NH₂-UiO-66(X) the use of different *d*⁰-metals of the same group, Ti⁴⁺, Zr⁴⁺ and Hf⁴⁺ is an obvious choice. While MOFs based on these ions have photocatalyzed reductions yielding solar fuels, the effect of the different electronic structure has not been unravelled, nor has a comparison of their photocatalytic activity been reported. However, the fundamental understanding of how properties and activity of these photocatalytic MOFs relate to each other, has the potential to move forward this field greatly.

In this study we focus on the electronic properties of NH₂-MIL-125(Ti), NH₂-UiO-66(Zr) and NH₂-UiO-66(Hf) and their influence on the photocatalytic performance in hydrogen evolution reaction (HER). For a fair comparison, the crystalline topology of these solids should be identical. These three structures were selected because of their clear similarities and the interest raised in the recent literature on their photocatalytic performance. In contrast to what has been recently reported, we demonstrate that only the Ti-based MOF exhibits appreciable catalytic activity while the frameworks of Zr and Hf are hardly active and exhibit nearly identical catalytic performance. Based on transient absorption spectroscopy, EPR and density functional theory (DFT), this difference is attributed to the nature of the excited states in these MOFs and emphasizes the importance of orbital contributions at the electronic 'band' edges.

Results and Discussion

NH₂-MIL-125(Ti) was synthesized by the protocol reported elsewhere^{27,51}. The synthesis yielded a material with high crystallinity and total pore volume⁷ (Table S1, Fig. S3).

The UiO-type materials are known to possess structural defects, as demonstrated by the non-stoichiometric metal to linker ratios observed by several groups experimentally. Here we synthesized two types of NH₂-UiO-66 that differ in the number of structural defects. They are denoted as X_d and X_i (X = Zr or Hf) and referred to as 'defective' and 'ideal', respectively. Based on the earlier works by Farha who reported the synthetic path yielding the defective UiO-66(Zr)²⁸, Lillerud claiming the nearly stoichiometric composition of the UiO obtained with the high temperature synthesis²⁹, and our own characterization, it can be safely assumed that the NH₂-UiO-66 materials used possess a different number of structural defects⁵¹. Zr_i has nearly a stoichiometric composition whereas Zr_d misses *ca.* 30% of linkers, in line with earlier observations by Farha *et al.*²⁸.

Figure 1c illustrates the N₂ adsorption isotherms for Ti, Zr_i and Hf_i expressed per mol of the corresponding metal showing the similarity of the three structures, two of which of the same topology (UiO).

Optical properties of the synthesized Ti-, Zr- and Hf-based MOFs were investigated by diffuse reflectance UV-Vis spectroscopy (Fig. 1d). In line with the previous reports, NH₂-MIL-125(Ti) possesses two absorption bands with the maxima at 280 and 382 nm^{7,15,30}. The lowest in energy absorption band tails up to 475 nm, covering a fraction of the visible part of the electromagnetic spectrum. This transition is ascribed to LMCT. The spectra of Zr_{i/d} and Hf_{i/d} are blue shifted as compared to that of Ti, exhibiting a similar spectral profile with two distinct absorption bands λ_{max} = 255 and 370 nm. Li and co-workers attributed the 370 nm absorption band to LMCT, analogously to the case of NH₂-MIL-125(Ti)²². They ascribed this absorption band to an *n*-π* transition of the linker and this excitation is followed by electron injection from a π* orbital to the zirconium core, in contrast to the claims of Matsuoka¹⁷.

The experimental HOCO-LUCO gap for NH₂-MIL-125 is 2.75 eV (Fig. S6), in good agreement with previous reports^{7,21,30}. On the other hand, the HOCO-LUCO gaps of Zr_i and Hf_i are identical and equal to 2.92 eV. Zr_d is at 2.95 eV and Hf_d is at 2.97 eV. While the HOCO-LUCO gaps of photocatalysts define the operation regime *i.e.* wavelength of light that can be utilized for chemical transformations, the absolute positions of HOCO and LUCO determine the thermodynamic feasibility of certain oxidations and reductions. To the best of our knowledge, the ionization potentials of NH₂-MIL-125(Ti) and NH₂-UiO-66(Zr or Hf) have not been reported to date.

Estimation of the heterogeneous H₂ redox potential is challenging, but applying the values determined in the solvated phase, we know this energy is near the vacuum level (*ca.* 4.4 eV). Considering only the energies of the frontier bands of the heterogeneous catalyst is not enough to predict the efficiency and activity of the material in the H₂ evolution reaction. From a purely thermodynamic perspective, the lower the electron affinity the greater the HER turnover should be. Thus, considering our computational findings⁵¹ depicted in Fig. 2, we would anticipate that the Zr- and Hf-MOFs should perform better than the Ti-material. However, we must also consider the identity of the orbitals that contribute to the frontier bands (LUCO).

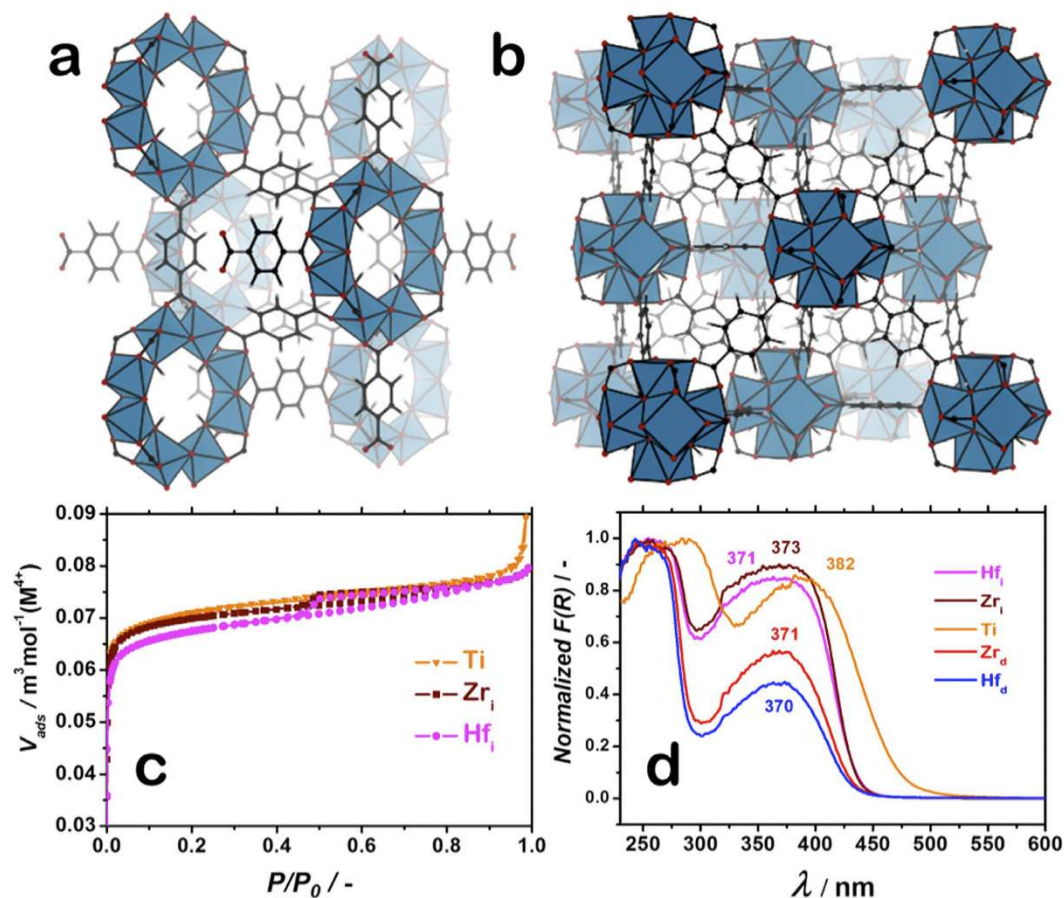


Figure 1. Structure and characterization of Metal-Organic Frameworks under investigation.

Representation of the crystallographic structures of NH₂-MIL-125(Ti) and NH₂-UiO-66(X) (where X = Zr and Hf) have the same crystal structures as their parent non-aminated frameworks, shown in (a,b), respectively; Nitrogen physisorption isotherms for the catalysts used in this work normalized to the mass of metal constituting the MOFs (c); Diffuse reflectance UV-Vis spectra of catalysts studied in Kubelka-Munk representation (d); NH₂-MIL-125(Ti) (orange), defective NH₂-UiO-66(Zr) (red), ideal NH₂-UiO-66(Zr) (bordeaux), defective NH₂-UiO-66(Hf) (blue), ideal NH₂-UiO-66(Hf) (magenta).

Indeed, Fig. 2 shows that the LUCO for the MIL-125 structure is centred on the TiO₂ (inorganic) region, whilst the two UiO-materials have a different electronic structure. Both the Zr- and Hf-materials have frontier band extrema located at the organics. This difference in the LUCO structure originates from the fact that the empty *d*-orbitals of Zr and Hf are too low in binding energy (close to the vacuum level) and thus do not overlap with the π^* orbital of the ligand despite the suitability of the geometrical arrangement of the orbitals. At the same time the *d*-orbitals of Ti fulfil both the spatial and energetic requirements, allowing for an efficient overlap. The DFT electronic structure infers that the single electron excited state of NH₂-MIL-125 should result in the formation of a delocalised Ti³⁺ species (which can localise by protonating a bridging oxide)²⁰, while no corresponding M³⁺ can be formed in the UiO structures. In the UiO series of materials, the organic-centred excitons are expected to be short-lived, although still some catalytic activity could be expected, since the thermodynamic energy level alignment is in favour of reducing H₂³¹.

In order to investigate the nature of excited states in the photocatalytic metal-organic frameworks we carried out electron paramagnetic resonance spectroscopy (EPR), shown in Fig. 3. The MOFs were subjected to conditions similar to those during photocatalytic reaction as described in the experimental part. In line with the previous reports^{17,18}, illuminating NH₂-MIL-125(Ti) with an energy corresponding to the HOCO-LUCO transition leads to the appearance of an intense paramagnetic signal ascribed to Ti³⁺^{13,17,18}. Most importantly, NH₂-UiO-66(Zr) and NH₂-UiO-66(Hf) exposed to the same conditions did not develop any additional paramagnetic features upon illumination. This result is in agreement with the data reported by Matsuoka and colleagues¹⁷. Most likely, if any paramagnetic species evolve as a result of irradiating the NH₂-UiO-66(X) solids, their lifetimes are too short for detection in the chosen experimental fashion.

So in principle, all MOFs subjected to the investigations have LUCO positions suitable to drive hydrogen evolution. In fact, the computational findings infer that Zr and Hf, when excited, possess an even greater thermodynamic driving force for accomplishing the desired reduction due to a lower electron affinity. However, reduction of the metal node only takes place in case of the Ti MOF.

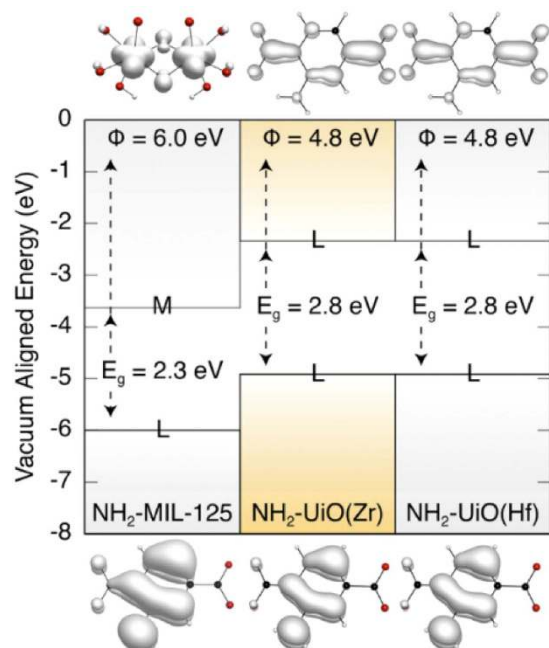


Figure 2. Electronic band alignment relative to the vacuum level of the three MOFs considered here from DFT calculations. Shown above and below are the orbitals contributing to the HOCO (*lower*) and LUCO (*upper*). M and L correspond to the localization of these orbitals on metal or ligand, respectively.

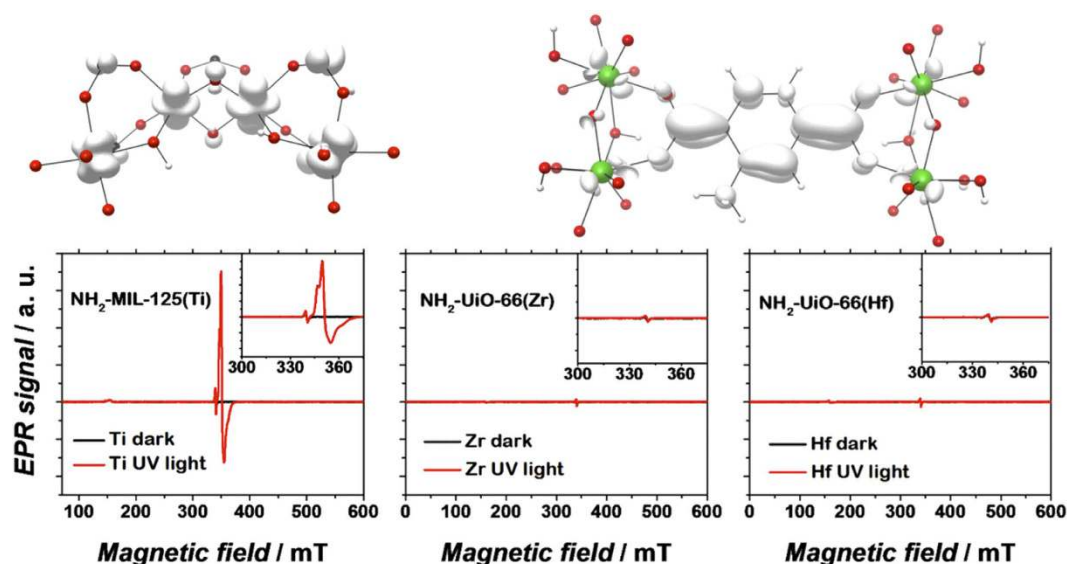


Figure 3. EPR spectra of dark (*black*) and UV-illuminated (*red*) MOFs: $\text{NH}_2\text{-MIL-125}(\text{Ti})$ (*left*), ‘ideal’ $\text{NH}_2\text{-UiO-66}(\text{Zr})$ (*centre*) and $\text{NH}_2\text{-UiO-66}(\text{Hf})$ (*right*). The photoexcited electron is primarily Ti-centred in the case of $\text{NH}_2\text{-MIL-125}$, whereas in the UiO-type materials, the electron resides on the organic linker.

The photocatalytic activity of the frameworks was assessed in visible light-driven hydrogen evolution. $\text{NH}_2\text{-MIL-125}(\text{Ti})$ clearly outperforms defective $\text{NH}_2\text{-UiO-66}(\text{Zr})$ and $\text{NH}_2\text{-UiO-66}(\text{Hf})$ (Fig. 4). The latter two have practically the same photocatalytic activity that is *ca.* 30 times lower than that of Ti. The rates of hydrogen evolution under visible light were determined by a linear fit of the hydrogen produced *vs.* time and found to be 49.3, 1, 1.7 and 1.7 $\mu\text{mol}\cdot\text{h}^{-1}\cdot\text{g}_{\text{catalyst}}$ for Ti, Zr_i, Hf_i, Zr_d and Hf_d, respectively. Titanium dioxide Degussa P25 was used as a benchmark and exhibited hydrogen evolution rate of 18.3 $\mu\text{mol}\cdot\text{h}^{-1}\cdot\text{g}_{\text{catalyst}}$ at the same reaction conditions. Stability of $\text{NH}_2\text{-MIL-125}(\text{Ti})$ ^{17,32}, $\text{NH}_2\text{-UiO-66}(\text{Zr})$ catalysts and their analogues²³ has been studied before and thus taken out of consideration. Interestingly, the defective samples exhibit an activity twice as high as the ideal ones and outperform them even when corrected for the amount of the corresponding metal (Table 1).

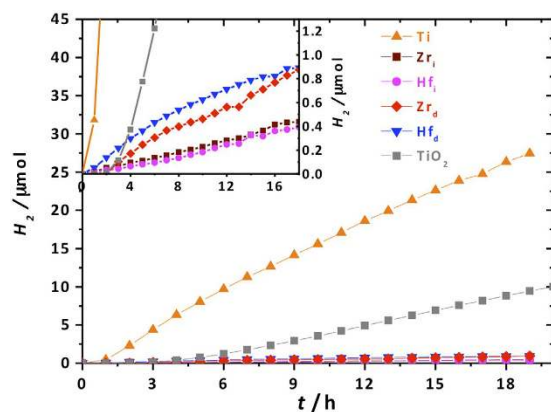


Figure 4. Photocatalytic performance of the MOF catalysts in hydrogen evolution: $\text{NH}_2\text{-MIL-125}(\text{Ti})$ (orange), defective $\text{NH}_2\text{-UiO-66}(\text{Zr})$ (red), ideal $\text{NH}_2\text{-UiO-66}(\text{Zr})$ (bordeaux), defective $\text{NH}_2\text{-UiO-66}(\text{Hf})$ (blue), ideal $\text{NH}_2\text{-UiO-66}(\text{Hf})$ (magenta), Degussa P25 (grey). The inset magnifies the region of interest for the UiO-type catalysts.

Sample	HOCO-LUCO gap/eV	Hydrogen evolution rate/ $\mu\text{mol}\cdot\text{h}^{-1}\cdot\text{g}_{\text{catalyst}}^{-1}$	Hydrogen evolution rate/ $\mu\text{mol}\cdot\text{h}^{-1}\cdot\text{mol}(\text{M}^{4+})^{-1}$	External quantum efficiency/%
Ti	2.75	49.3	12747	0.022
Zr_i	2.92	1	357 ^a	0.0009
Hf_i	2.92	1	467 ^a	0.0009
Zr_d	2.95	1.7	472 ^b	0.0016
Hf_d	2.97	1.7	654 ^b	0.0016

Table 1. Catalytic performance. ^aStoichiometric crystal composition: $\text{M}^{4+}:\text{ATA} = 1:1$. ^bDefective crystals: $\text{M}^{4+}:\text{ATA} = 3:2$.

This difference in photocatalytic performance may originate from (i) a substantially smaller particle size of the defective solids and thus a larger external surface; (ii) a larger BET area; (iii) a positive influence of the defects on the kinetics of photocatalysis.

The first reasoning is particularly important in the case of dense oxides where chemical reactions can only occur at the surface of photocatalyst particles. However, we expect that in the case of MOFs this argument is of minor importance unless bulky substrates are subjected to photocatalysis. At first sight the second scenario seems the most logical: the BET area of the defective catalysts is much larger than the one of ideal MOFs. While this is true for Zr_d vs. Zr_i , the case of $\text{NH}_2\text{-UiO-66}(\text{Hf})$ suggests that the main contribution to the catalytic performance is not the difference in surface areas. The BET areas of Hf_d and Hf_i are 789 and 706 m^2g^{-1} respectively. Such small difference should not account for doubling the catalytic rate. The difference in optical properties is also negligible when speaking of such rate enhancement. In fact, the external quantum efficiencies of defective solids are twice as high as the ones of ideal MOFs as summarized in Table 1. This suggests that the structural defects within the UiO-type solids improve the hydrogen evolution rate³³.

As already anticipated, the observed difference in activity between the Ti and the Hf, Zr catalysts can only be explained by the location of the LUCO at the inorganic node in case of $\text{NH}_2\text{-MIL-125}(\text{Ti})$. Indeed, even taking into account the difference in optical properties, $\text{NH}_2\text{-MIL-125}(\text{Ti})$ achieves an external quantum efficiency (EQE) ca. 13 times larger than the one of defective $\text{NH}_2\text{-UiO-66}(\text{Zr})$ (Table 1). In order to further prove this hypothesis, transient absorption spectroscopy (TAS) was applied to study the lifetime of the excited states in these solids.

Results are presented in Fig. 5. The MOFs were excited at the wavelengths correspond corresponding to their respective absorption maxima. Excitation of $\text{NH}_2\text{-MIL-125}(\text{Ti})$ results in an intense transient signal with a maximum at 560 and 600 nm, and a very broad peak from <500 nm till over 860 nm. A transient kinetic model with three consecutively decaying states was necessary to obtain a reasonable fit for the experimental data^{34,SI}. The third transient state has a moderately long lifetime of up to 9 ns (Table 2).

The transient spectra of $\text{NH}_2\text{-UiO-66}(\text{Zr})$ and $\text{NH}_2\text{-UiO-66}(\text{Hf})$ are markedly different from the one of Ti. The transient signals of Zr_i and Hf_i are nearly identical in terms of both decay kinetics and the spectral signatures^{SI}. Right after the laser pulse, a broad transient signal emerges at 750 nm and decays rapidly to the ground state. The lifetime of this signal is 1.5 ps in both cases.

The defective solids exhibit a different behaviour. First of all, a transient kinetic model with three consecutive states, after which the material decays to the ground state, was necessary to obtain a reasonable fit for the experimental data (see SI)³⁴. Moreover, the transient absorption band is shifted to shorter wavelengths compared to the ones of Zr_i and Hf_i . The excited states of Hf_d and Zr_d have significantly longer lifetimes up to 190 and 130 ps, respectively. So, these samples have distinct properties different from Zr_i and Hf_i . In addition to the rapid decay

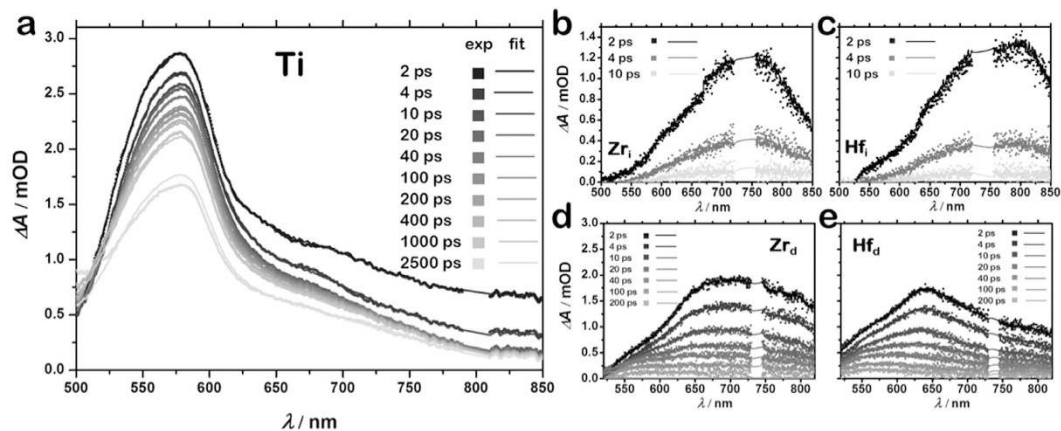


Figure 5. Transient absorption spectroscopy. Differential transient absorption spectra for $\text{NH}_2\text{-MIL-125(Ti)}$ upon excitation at 400 nm (a); Differential transient absorption spectra for 'ideal' (b) and 'defective' (d) $\text{NH}_2\text{-UiO-66(Zr)}$ and 'ideal' (c) and 'defective' (e) $\text{NH}_2\text{-UiO-66(Hf)}$ upon excitation at 370 nm. Symbols represent experimental data and lines the fits.

Sample	Lifetime of transient signal/ps		
	1.6	80	$9 \cdot 10^3$
Ti	1.6	80	$9 \cdot 10^3$
Hf_d	2.4	20	190
Zr_d	1.6	10	130
Hf_i	1.4	-	-
Zr_i	1.5	-	-

Table 2. Fitting parameters of the transient absorption spectra for the MOF-catalysts.

pathway registered in the case of ideal crystals, the defective Zr_d and Hf_d also undergo a relaxation pathway with longer lifetimes, although still two orders of magnitude shorter than the ones of Ti (Table 2).

Based on the EPR data and the computational results, the transient signals in the case of Hf and Zr structures can be assigned to the HOCO-LUCO transition of the $\text{NH}_2\text{-UiO-66(X)}$ framework. This transition is purely ligand-based and is independent of the metal ion employed. In contrast, in the Ti MOF, as established by EPR, Ti^{3+} is generated upon illumination. The main difference between the Zr/Hf and the Ti transient spectra, is the occurrence of absorption bands at much lower wavelengths in $\text{NH}_2\text{-MIL-125(Ti)}$, namely 560 and 600 nm, assigned to the stabilisation of the hole over the organic linker³⁵, in contrast to earlier works where absorbance of similar materials with photo-generated Ti^{3+} occurs in the 500–600 nm range and is usually assigned to such Ti^{3+} species^{36,37}.

These results are in line with the photocatalytic experiments. Indeed, a more efficient photocatalysis is expected when photo-excited charges have a longer lifetime. The longer lifetime for the $\text{NH}_2\text{-MIL-125(Ti)}$ with respect to the $\text{NH}_2\text{-UiO-66(Zr)}$ and $\text{NH}_2\text{-UiO-66(Hf)}$ is also in accordance with the EPR and DFT results. For MOFs where the lowest energy transition resides purely at the organic linker, as opposed to a LMCT, the lifetime of excited states is too short as to allow for efficient utilization of the photogenerated electrons. Such long-lived LMCT can be achieved when the energy of metal orbitals is close to the one of the π^* -orbital of the organic linker thus allowing for an efficient overlap. In the case of aminoterephthalate, Ti appears to be an excellent metal. However, even metal ions with lower binding energies can potentially be utilized in this fashion as long as the appropriate linker is concerned.

Conclusions

The photocatalytic potential of the group IV d^0 metal-based metal-organic frameworks $\text{NH}_2\text{-MIL-125(Ti)}$, $\text{NH}_2\text{-UiO-66(Zr)}$ and $\text{NH}_2\text{-UiO-66(Hf)}$ was explored. First-principles electronic structure theory indicates that each of these MOFs has a LUCO position suitable for driving the hydrogen evolution reaction. However, experimentally the visible light photocatalytic activity of $\text{NH}_2\text{-MIL-125(Ti)}$ is much higher than the UiO MOFs. This remarkable difference can be understood in terms of the kinetics of the corresponding photoexcited states. While the LMCT excited state of $\text{NH}_2\text{-MIL-125(Ti)}$ is stabilized by the formation of Ti^{3+} , excitation of $\text{NH}_2\text{-UiO-66(Zr)}$ and $\text{NH}_2\text{-UiO-66(Hf)}$ does not promote the formation of corresponding M^{3+} as is evident from the DFT and EPR studies. In contrast to $\text{NH}_2\text{-MIL-125(Ti)}$, the HOCO-LUCO transitions of $\text{NH}_2\text{-UiO-66(X)}$ are purely ligand-based and have a short lifetime accounting for the poor catalytic performance. The d -orbitals of Zr and Hf are too close to the vacuum level (low electron affinity) and do not overlap with the π^* orbital of the ligand despite their geometrical suitability. Structural defects of the UiO MOFs result in twice higher catalytic rates due to the longer lifetime of the photoexcited states.

This work signifies the importance of the identity of orbitals defining the band extrema. The LMCT excited state of $\text{NH}_2\text{-MIL-125}(\text{Ti})$ has a superior lifetime as compared to the organic-based states of the UiOs. The design of MOF for photocatalysis should focus on sufficiently long excited state lifetimes, thus improving catalytic activity.

Experimental

Materials and reagents. All chemicals were purchased from Sigma Aldrich and used without further purification. Methanol and dimethylformamide (DMF) were additionally dried over molecular sieve (zeolite 5 Å).

Syntheses. *$\text{NH}_2\text{-MIL-125}(\text{Ti})$* . The MOF was synthesized using the protocol reported by Moreira and co-workers²⁷. In a typical synthesis, 2.86 g (15.8 mmol) of 2-aminoterephthalic acid was dissolved in a mixture of 40 mL dry N, N-dimethylformamide (DMF) and 10 mL dry methanol (at room temperature). Then 2.86 mL (9.7 mmol) of titanium isopropoxide were added and the mixture was placed in an autoclave. The autoclave was sealed and the mixture was heated for 72 h at 110 °C. The obtained yellow solid was filtered, dispersed in fresh DMF and kept under stirring overnight (50 mL DMF per 1 g product) in order to remove residual linker. Then, the same procedure was repeated twice using methanol instead of DMF to exchange the DMF within the pores. The solid was finally dried under air at 100 °C.

$\text{NH}_2\text{-UiO-66}(\text{Zr/Hf})$ 'defective'. The protocol is based on the procedure reported by Farha and co-workers²⁸. For the synthesis of $\text{NH}_2\text{-UiO-66}(\text{X})$, where X = Zr or Hf, ZrCl_4 (250 mg) or HfCl_4 (346 mg) were dissolved in DMF (10 mL) in the presence of concentrated HCl (2 mL) upon sonication. Additional DMF (15 mL) and 2-aminoterephthalic acid (268 mg) were introduced and the mixture was placed in an autoclave and heated overnight at 80 °C. The pale yellow solids were filtered off, suspended in DMF and sonicated for 10 min. This procedure was repeated twice with DMF and then twice with methanol. The solid was dried under air at 100 °C.

$\text{NH}_2\text{-UiO-66}(\text{Zr/Hf})$ 'ideal'. These MOFs were synthesized following the protocol reported by Lillerud *et al.*²⁹ ZrCl_4 (945 mg) or HfCl_4 (1.308 g) were dissolved in DMF (24.4 mL) in the presence of concentrated HCl (0.7 mL) upon sonication. 1.467 g of 2-aminoterephthalic acid were introduced and the mixture was then heated for 20 h at 220 °C in an autoclave. The pale yellow precipitate was filtered off and washed twice with DMF at 100 °C (10 h each), then methanol at 100 °C (10 h each).

Characterization. *Powder X-Ray diffraction* patterns were recorded using Bruker-AXS D5005 with $\text{Co-K}\alpha$ radiation.

N_2 -physisorption experiments were carried out at 77 K in a TriStar II unit gas adsorption analyser (Micromeritics). Prior to the measurements the samples were degassed at 423 K under vacuum for 16 h. The BET areas were calculated using intervals allowing positive BET constants³⁸. The total pore volumes were calculated at 0.9 relative pressure.

Scanning electron microscopy (SEM) was carried out using a JEOL JSM-6010LA InTouchScope microscope.

Thermogravimetric analysis was performed by means of Mettler Toledo TGA/SDTA851e, under an air flow of 60 ml min^{-1} at a heating rate of 10 K min^{-1} up to 1073 K.

Diffuse reflectance UV/Vis spectra were collected using a Perkin-Elmer Lambda 900 spectrophotometer equipped with an integrating sphere ("Labsphere") in the 200–800 nm range. BaSO_4 was used as a white standard.

EPR spectroscopy. Steady-state EPR measurements were carried out at X-band (9.52 GHz) using a commercial EPR spectrometer Bruker Elexsys E580 equipped with an Oxford Instruments temperature control system ($T = 4\text{--}300\text{ K}$). All spectra were acquired at 40 K. Samples were prepared by suspending 25 mg MOF in a solution of electron donor triethylamine (TEA)/ $\text{CH}_3\text{CN}/\text{H}_2\text{O} = 1/5/0.1$ (total volume 200 μL). The volume of suspension placed into the EPR resonator was 50–60 μL . Each sample was degassed by several freeze-pump-thaw procedures and then sealed in an EPR quartz tube (OD 3.8 mm, ID 2.8 mm). When needed, the samples were exposed to a 500 W mercury lamp equipped with an IR filter (H_2O , 7 cm optical path) and a UFS6 filter (see Fig. S7) for 30 min. After this period the sample tube was placed into liquid nitrogen. The cool-down time to frozen state was ~10–15 s. Then it was inserted into EPR cryostat.

Femtosecond Transient Absorption Spectroscopy. Samples were excited using 180 fs pulses at 400 nm for $\text{NH}_2\text{-MIL-125}(\text{Ti})$ and 370 nm for $\text{NH}_2\text{-UiO-66}(\text{Zr})$ and $\text{NH}_2\text{-UiO-66}(\text{Hf})$ generated in a YKGBW oscillator (Light Conversion, Pharos SP) at 1028 nm through nonlinear frequency mixing in an OPA and second harmonics module (Light Conversion, Orpheus). A small fraction of the 1028 nm fundamental beam was split off to generate the broadband probe spectrum in a sapphire (500–1600 nm) crystal. The probe pulse was delayed relative to the pump using a delay stage with maximum delay of 3 ns. The pump and probe pulses overlap on the sample position under an angle of ~8 degrees, after which the probe light is led to a detector suitable for the probe spectrum selected (Ultrafast Systems, Helios). In order to prevent multiple photons absorption processes, the pump fluence was set sufficiently low, allowing us to study single exciton dynamics. In a typical experiment 2.7 mg MOF was dispersed in acetonitrile (700 μL) and sonicated for 30 min. In order to separate large particles (>100 nm), the suspension was then centrifuged for 8 min at 10000 rpm. The supernatant was placed in a 2 mm stirred quartz cuvette for the measurements. Transient data were analyzed using a global fitting routine in which the spectral evolution of the time-dependent absorption difference spectra is fitted to a sequential model yielding evolution-associated difference spectra (EADS)³⁹. In the case of the $\text{NH}_2\text{-MIL-125}(\text{Ti})$ and $\text{NH}_2\text{-UiO-66}(\text{Zr/Hf})$ 'defective' a three-state kinetic model was used to fit the experimental data³⁴. An additional state was used to force the system to decay to the ground state. All time traces were satisfactorily fitted with three time constants. The

last state decays to the ground state being part of the model. For the $\text{NH}_2\text{-UiO-66}(\text{Zr}/\text{Hf})$ ‘ideal’ one excited state (which population’s decay is defined by $\exp(-k\tau)$) that goes to the ground state (described by $\{1 - \exp(-k\tau)\}$) was sufficient for a good fit.

Computational Methods. All calculations were performed within the framework of density functional theory with electron exchange and correlation treated with the semi-local PBEsol functional (for structure relaxation) and the non-local screened HSE06 functional (for quantitative electronic structure information). The crystalline MOFs were described within periodic boundary conditions are implemented in the VASP computational chemistry package⁴⁰. A 500 eV planewave cut-off and Gamma point sampling of the first Brillouin zone was found to be sufficient for energy convergence within 0.01 eV per atom. Starting with experimentally collected crystallographic structures, lattice parameters and atomic positions were relaxed with PBEsol to equilibrium structures, which are available in an external data repository: https://github.com/WMD-Bath/Crystal_Structures. The optimized structures were then computed with HSE06 to recover the electronic structure. Electron energies were aligned to the vacuum level using a procedure developed by Butler, Hendon and Walsh, and the code is freely available²⁴. A model of the triplet state (*i.e.* a first excited state) was obtained by fixing the total spin moment in the crystallographic unit cell (NUPDOWN = 2 in VASP). Images were made in VESTA⁴¹.

Photocatalytic studies. Photocatalytic experiments were carried out using a home-built set-up equipped with a 500 W Xe/Hg lamp (66983, Newport). It consists of a custom-made Pyrex-glass reactor, a CP 9001 gas chromatograph (Chrompack) for analysis of the headspace, a KSLA gas pump and the light source. Light intensity was measured with AvaSpec-3648-2-USB2 (Avantes, the Netherlands). The reactor has a volume of 42.1 mL and is equipped with a water jacket to allow for precise temperature control. The light emitted by the lamp passes through a lens assembly (77330, Newport) focusing the beam on the reactor window, an H_2O filter (61945, Newport) and a 385 nm cut-off optical filter. The pump is applied to ensure a sufficient mixing of gases in the headspace of the reactor and the stainless steel tubes (2.5 mL/min continuous operation). Every 60 min a probe of the headspace is analyzed by the GC. In a typical experiment 30 mg of a MOF were suspended in 23.5 mL of CH_3CN , 4.7 mL of TEA and 0.5 mL of H_2O . The suspension was then placed in the reactor and deoxygenated by an argon flow of 30 mL/min applied for 30 min at 25 °C. The oxygen concentration was monitored by the GC analysis. Once the system became free of oxygen, the illumination was applied followed by the GC analysis. All the visible light photocatalytic experiments were carried out at 40 °C monitored by a thermocouple. The heat was supplied in order to maximize the hydrogen production allowing the detection of H_2 gas in the case of samples with the lowest activity.

References

- Rodenas, T. *et al.* Metal–organic framework nanosheets in polymer composite materials for gas separation. *Nat Mater* **14**, 48–55, doi: 10.1038/nmat4113 (2015).
- Seoane, B. *et al.* Metal–organic framework based mixed matrix membranes: a solution for highly efficient CO_2 capture? *Chemical Society Reviews* **44**, 2421–2454, doi: 10.1039/C4CS00437J (2015).
- Gascon, J., Corma, A., Kapteijn, F. & Llabrés i Xamena, F. X. Metal Organic Framework Catalysis: Quo vadis? *ACS Catalysis* **4**, 361–378, doi: 10.1021/cs400959k (2014).
- Butler, K. T., Hendon, C. H. & Walsh, A. Electronic Structure Modulation of Metal–Organic Frameworks for Hybrid Devices. *ACS Applied Materials & Interfaces* **6**, 22044–22050, doi: 10.1021/am507016r (2014).
- Llabrés i Xamena, F. X., Corma, A. & Garcia, H. Applications for Metal–Organic Frameworks (MOFs) as Quantum Dot Semiconductors. *The Journal of Physical Chemistry C* **111**, 80–85, doi: 10.1021/jp063600e (2006).
- Alvaro, M., Carbonell, E., Ferrer, B., Llabrés i Xamena, F. X. & Garcia, H. Semiconductor behavior of a metal–organic framework (MOF). *Chemistry – A European Journal* **13**, 5106–5112, doi: 10.1002/chem.200601003 (2007).
- Nasalevich, M. A., Goesten, M. G., Savenije, T. J., Kapteijn, F. & Gascon, J. Enhancing optical absorption of metal–organic frameworks for improved visible light photocatalysis. *Chemical Communications* **49**, 10575–10577, doi: 10.1039/C3CC46398B (2013).
- Zhang, T. & Lin, W. Metal–organic frameworks for artificial photosynthesis and photocatalysis. *Chemical Society Reviews* **43**, 5982–5993, doi: 10.1039/C4CS00103F (2014).
- Long, J. *et al.* Amine-functionalized zirconium metal–organic framework as efficient visible-light photocatalyst for aerobic organic transformations. *Chemical Communications* **48**, 11656–11658, doi: 10.1039/c2cc34620f (2012).
- Wang, C.-C., Li, J.-R., Lv, X.-L., Zhang, Y.-Q. & Guo, G. Photocatalytic organic pollutants degradation in metal–organic frameworks. *Energy & Environmental Science* **7**, 2831–2867, doi: 10.1039/C4EE01299B (2014).
- Shen, L., Liang, S., Wu, W., Liang, R. & Wu, L. Multifunctional NH_2 -mediated zirconium metal–organic framework as an efficient visible-light-driven photocatalyst for selective oxidation of alcohols and reduction of aqueous $\text{Cr}(\text{vi})$. *Dalton Transactions* **42**, 13649–13657, doi: 10.1039/C3DT51479J (2013).
- Wang, J. L., Wang, C. & Lin, W. Metal–organic frameworks for light harvesting and photocatalysis. *ACS Catalysis* **2**, 2630–2640, doi: 10.1021/cs3005874 (2012).
- Dan-Hardi, M. *et al.* A new photoactive crystalline highly porous titanium(IV) dicarboxylate. *Journal of the American Chemical Society* **131**, 10857–10859, doi: 10.1021/ja903726m (2009).
- Cavka, J. H. *et al.* A New Zirconium Inorganic Building Brick Forming Metal Organic Frameworks with Exceptional Stability. *Journal of the American Chemical Society* **130**, 13850–13851, doi: 10.1021/ja8057953 (2008).
- Fu, Y. *et al.* An amine-functionalized titanium metal–organic framework photocatalyst with visible-light-induced activity for CO_2 reduction. *Angewandte Chemie – International Edition* **51**, 3364–3367, doi: 10.1002/anie.201108357 (2012).
- Nasalevich, M., van der Veen, M. A., Kapteijn, F. & Gascon, J. Metal–Organic Frameworks as heterogeneous photocatalysts: advantages and challenges. *CrystEngComm*, doi: 10.1039/C4CE00032C (2014).
- Horiuchi, Y. *et al.* Visible-light-promoted photocatalytic hydrogen production by using an amino-functionalized Ti(IV) metal–organic framework. *Journal of Physical Chemistry C* **116**, 20848–20853, doi: 10.1021/jp3046005 (2012).
- Nasalevich, M. A. *et al.* $\text{Co@NH}_2\text{-MIL-125}(\text{Ti})$: cobaloxime-derived metal–organic framework-based composite for light-driven H_2 production. *Energy & Environmental Science* **8**, 364–375, doi: 10.1039/C4EE02853H (2015).
- De Miguel, M. *et al.* Evidence of photoinduced charge separation in the metal–organic framework $\text{MIL-125}(\text{Ti})\text{-NH}_2$. *ChemPhysChem* **13**, 3651–3654, doi: 10.1002/cphc.201200411 (2012).

20. Walsh, A. & Catlow, C. R. A. Photostimulated Reduction Processes in a Titania Hybrid Metal–Organic Framework. *ChemPhysChem* **11**, 2341–2344, doi: 10.1002/cphc.201000306 (2010).
21. Hendon, C. H. *et al.* Engineering the Optical Response of the Titanium–MIL-125 Metal–Organic Framework through Ligand Functionalization. *Journal of the American Chemical Society*, doi: 10.1021/ja405350u (2013).
22. Sun, D. *et al.* Studies on Photocatalytic CO₂ Reduction over NH₂-UiO-66(Zr) and Its Derivatives: Towards a Better Understanding of Photocatalysis on Metal–Organic Frameworks. *Chemistry—A European Journal* **19**, 14279–14285, doi: 10.1002/chem.201301728 (2013).
23. Sun, D., Liu, W., Qiu, M., Zhang, Y. & Li, Z. Introduction of a mediator for enhancing photocatalytic performance via post-synthetic metal exchange in metal–organic frameworks (MOFs). *Chemical Communications* **51**, 2056–2059, doi: 10.1039/C4CC09407G (2015).
24. Butler, K. T., Hendon, C. H. & Walsh, A. Electronic Chemical Potentials of Porous Metal–Organic Frameworks. *Journal of the American Chemical Society* **136**, 2703–2706, doi: 10.1021/ja4110073 (2014).
25. Hammett, L. P. The Effect of Structure upon the Reactions of Organic Compounds. Benzene Derivatives. *Journal of the American Chemical Society* **59**, 96–103, doi: 10.1021/ja01280a022 (1937).
26. Lee, Y., Kim, S., Kang, J. K. & Cohen, S. M. Photocatalytic CO₂ reduction by a mixed metal (Zr/Ti), mixed ligand metal–organic framework under visible light irradiation. *Chemical Communications* **51**, 5735–5738, doi: 10.1039/C5CC00686D (2015).
27. Moreira, M. A. *et al.* Effect of ethylbenzene in p-xylene selectivity of the porous titanium amino terephthalate MIL-125(Ti)-NH₂. *Microporous and Mesoporous Materials* **158**, 229–234, doi: 10.1016/j.micromeso.2012.03.039 (2012).
28. Katz, M. J. *et al.* A facile synthesis of UiO-66, UiO-67 and their derivatives. *Chemical Communications* **49**, 9449–9451, doi: 10.1039/C3CC46105J (2013).
29. Shearer, G. C. *et al.* Tuned to Perfection: Ironing Out the Defects in Metal–Organic Framework UiO-66. *Chemistry of Materials* **26**, 4068–4071, doi: 10.1021/cm501859p (2014).
30. Nasalevich, M. A., Goesten, M. G., Savenije, T. J., Kapteijn, F. & Gascon, J. Correction: Enhancing optical absorption of metal–organic frameworks for improved visible light photocatalysis. *Chemical Communications* **51**, 961–962, doi: 10.1039/C4CC90482F (2015).
31. Hendon, C. H. & Walsh, A. Chemical principles underpinning the performance of the metal–organic framework HKUST-1. *Chemical Science* **6**, 3674–3683, doi: 10.1039/C5SC01489A (2015).
32. Toyao, T. *et al.* Efficient hydrogen production and photocatalytic reduction of nitrobenzene over a visible-light-responsive metal–organic framework photocatalyst. *Catalysis Science & Technology* **3**, 2092–2097, doi: 10.1039/C3CY00211J (2013).
33. Fang, Z. L., Bueken, B., De Vos, D. E. & Fischer, R. A. Defect-Engineered Metal–Organic Frameworks. *Angewandte Chemie-International Edition* **54**, 7234–7254, doi: 10.1002/anie.201411540 (2015).
34. Hunger, J. *et al.* Hydrogen-Bond Dynamics in a Protic Ionic Liquid: Evidence of Large-Angle Jumps. *The Journal of Physical Chemistry Letters* **3**, 3034–3038, doi: 10.1021/jz301334j (2012).
35. Santaclara, J. G., Nasalevich, M. A., Castellanos, S., Evers, W. H., Spoor, F. C. M., Rock, K., Siebbeles, L. D. A., Kapteijn, F., Grozema, F., Houtepen, A., Gascon, J., Hunger, J. & van der Veen, M. A. Organic linker defines the excited-state decay of photocatalytic MIL-125(Ti)-type materials. *ChemSusChem* **9**, 388–395, doi: 10.1002/cssc.20150135 (2006).
36. Kameneva, O. *et al.* New photoactive hybrid organic–inorganic materials based on titanium–oxo-PHEMA nanocomposites exhibiting mixed valence properties. *Journal of Materials Chemistry* **15**, 3380–3383, doi: 10.1039/B507305G (2005).
37. Kuznetsov, A. I. *et al.* Laser-induced photopatterning of organic–inorganic TiO₂-based hybrid materials with tunable interfacial electron transfer. *Physical Chemistry Chemical Physics* **11**, 1248–1257, doi: 10.1039/B814494J (2009).
38. De Lange, M. F., Vlugt, T. J. H., Gascon, J. & Kapteijn, F. Adsorptive characterization of porous solids: Error analysis guides the way. *Microporous and Mesoporous Materials* **200**, 199–215, <http://dx.doi.org/10.1016/j.micromeso.2014.08.048> (2014).
39. van Stokkum, I. H. M., Larsen, D. S. & van Grondelle, R. Erratum to “Global and target analysis of time-resolved spectra” [*Biochimica et Biophysica Acta* 1658/2–3 (2004) 82–104]. *Biochimica et Biophysica Acta (BBA)—Bioenergetics* **1658**, 262, <http://dx.doi.org/10.1016/j.bbabi.2004.08.005> (2004).
40. Kresse, G. & Furthmüller, J. Efficient iterative schemes for \textit{ab initio} total-energy calculations using a plane-wave basis set. *Physical Review B* **54**, 11169–11186 (1996).
41. Momma, K. & Izumi, F. VESTA 3 for three-dimensional visualization of crystal, volumetric and morphology data. *Journal of Applied Crystallography* **44**, 1272–1276, doi: 10.1107/S0021889811038970 (2011).

Acknowledgements

Dr. Sonia Castellanos Ortega is gratefully acknowledged for scanning electron microscopy. The Dutch National Research School Combination Catalysis Controlled by Chemical Design (NRSC-Catalysis) is acknowledged for funding the work at Delft. The work at Bath was supported by the European Research Council (Starting Grant 277757), and access to ARCHER through membership in the UK’s HPC Materials Chemistry Consortium, which is funded by EPSRC (Grant No. EP/L00202). S.L.V. and M.V.F. thank the Russian Science Foundation (no. 14-13-00826).

Author Contributions

The experiments were designed by M.A.N. and J.G. F.K. and J.G. directed the research. M.A.N. carried out the synthesis and basic characterization of all catalysts and measured their catalytic performance with assistance from B.vd.L. C.H.H., K.S. and A.W. designed and carried out the DFT calculations. J.G.S., A.J.H. and M.A.vd.V. carried out and interpreted the fast spectroscopy characterization. M.V.F. and S.L.V. performed and interpreted the EPR experiments. The manuscript with primarily written by M.A.N. and J.G. with contributions from all authors.

Additional Information

Supplementary information accompanies this paper at <http://www.nature.com/srep>

Competing financial interests: The authors declare no competing financial interests.

How to cite this article: Nasalevich, M. A. *et al.* Electronic origins of photocatalytic activity in *d*⁰ metal organic frameworks. *Sci. Rep.* **6**, 23676; doi: 10.1038/srep23676 (2016).



This work is licensed under a Creative Commons Attribution 4.0 International License. The images or other third party material in this article are included in the article’s Creative Commons license, unless indicated otherwise in the credit line; if the material is not included under the Creative Commons license, users will need to obtain permission from the license holder to reproduce the material. To view a copy of this license, visit <http://creativecommons.org/licenses/by/4.0/>